



## Research paper

# Carboniferous bentonites from 10Th Khutor deposit (Russia): Composition, properties and features of genesis

P. Belousov<sup>a,\*</sup>, N. Chupalenkov<sup>b</sup>, G.E. Christidis<sup>c</sup>, O. Zakusina<sup>a</sup>, S. Zakusin<sup>a,d</sup>, I. Morozov<sup>a</sup>, M. Chernov<sup>d</sup>, T. Zaitseva<sup>e</sup>, E. Tyupina<sup>f,g</sup>, V. Krupskaya<sup>a,d,h</sup>

<sup>a</sup> Institute of Geology of Ore Deposits, Petrography, Mineralogy and Geochemistry, Russian Academy of Science (IGEM RAS), Staromonetny per. 35, Moscow 119017, Russian Federation

<sup>b</sup> Federal State Budgetary Institution "All-Russian Scientific-research Institute of Mineral Resources named after N.M.Fedorovsky, Staromonetny per. 31, Moscow 119017, Russian Federation

<sup>c</sup> Technical University of Crete, School of Mineral Resources Engineering, 73100 Chania, Crete, Greece

<sup>d</sup> Lomonosov Moscow State University, Geological Faculty, Leninskie Gory 1, Moscow 119991, Russian Federation

<sup>e</sup> Institute of Precambrian Geology and Geochronology, Russian Academy of Sciences (IPGG RAS), nab. Makarova 2, St. Petersburg 199034, Russian Federation

<sup>f</sup> D. Mendeleev University of Chemical Technology of Russia, Department of High Energy Chemistry and Radioecology, Miusskaya sq. 9, Moscow 125047, Russian Federation

<sup>g</sup> National Research Nuclear University «MEPhI», Department of Closed Nuclear Fuel Cycle Technology, Kashirskoe highway 31, Moscow 115409, Russian Federation

<sup>h</sup> Nuclear Safety Institute, Russian Academy of Science (IBRAE RAS), 2nd Tul'sky lane, 2/52, Moscow 115191, Russian Federation



## ARTICLE INFO

## Keywords:

Bentonite  
Montmorillonite  
Genesis  
Volcano-sedimentary rocks  
Diagenetic alteration  
Volcanic glass

## ABSTRACT

This article studies the geological structure, mineralogical composition, genesis and industrial properties of bentonite of the 10th Khutor deposit (Republic of Khakassia, Russia). The deposit is confined to the coal-bearing formation of Carboniferous age and is one of the main sources of bentonite for the metallurgical and foundry industries in Russia. The samples were collected during several field seasons and were studied with XRD, SEM, DTA, XRF, FTIR, BET and CEC analysis. The deposit consists of 6 productive layers with montmorillonite of alkaline-earth type varying in content from 38 to 72%. The formation of bentonites is associated with the alteration of volcanic ash of rhyodacite and dacite composition in zones of shallow sea water - bays and lagoons. The specific conditions of the formation, like an evaporitic depositional environment with high concentrations of soluble salts and burial diagenesis, as evidenced by seams and packs of hard coal, affected the textural and surface properties of the bentonite and caused the observed low microporosity and limited illitization.

## 1. Introduction

The estimated reserves of bentonites in Russia are 185 million tons (Belousov and Krupskaya, 2019; State balance of mineral reserves of the Russian Federation: Bentonite Clays, 2018). In terms of consumption, the most important consumers of bentonite in Russia are mining and processing plants, foundries and drilling companies. Also, bentonite is used in civil engineering, in the production of cat litter, medicine, cosmetology and other industries in Russia. Currently, a new direction actively developing in Russia is the construction of engineered barrier systems for the disposal of radioactive waste in deep geological repository the Yeniseiskiy site (Krupskaya et al., 2018, 2020; Iliina et al., 2019). All large Russian bentonite deposits are confined to plates and platforms, orogenic belts and foredeeps and are mainly of sedimentary

and diagenetic origin (Belousov and Krupskaya, 2019).

The annual production of bentonite in Russia is ~700 thousand tons (Belousov and Krupskaya, 2019). The 10th Khutor deposit is located in Siberia, 8 km southwest of the city of Chernogorsk (Republic of Khakassia, Russia) and is the main source of bentonite in Russia, with an annual production of about 300 thousand tons. The first reports on the deposit appeared in 1959, when, as a result of geological exploration, 12 million tons of clays for drilling fluids were put on the balance. However, active mining began only in the early 2000s. By now, the reserves of the deposit are slightly less than 2 million tons. Due to its quality characteristics, the main consumers of bentonite products are foundries and ore mining and processing plants. In connection with active development, at the moment, the exploration and commissioning of two neighboring deposits located in close proximity to 10th Khutor

\* Corresponding author.

E-mail address: [belousov.peter@list.ru](mailto:belousov.peter@list.ru) (P. Belousov).

<https://doi.org/10.1016/j.clay.2021.106308>

Received 12 March 2021; Received in revised form 5 October 2021; Accepted 13 October 2021

Available online 23 October 2021

0169-1317/© 2021 The Authors. Published by Elsevier B.V. This is an open access article under the CC BY license (<http://creativecommons.org/licenses/by/4.0/>).



Despite the detailed exploration of the 10th Khutor deposit in previous periods, studies of the genesis of bentonites and structural features of montmorillonites have not yet been carried out. The main purpose of this work was to establish the conditions for the formation of this deposit, as well as to study the features of the mineral composition and physicochemical properties of these raw materials. In addition to fundamental issues, the aim of the work is to assess the properties and quality of the bentonite beds.

## 2. Regional geology and geology of the 10th Khutor bentonite deposit

### 2.1. Overall geology

In the Republic of Khakassia, bentonite distribution is confined to the areas with a continental tuff-sandy- argillaceous formation of Carboniferous age of the Yuzhno-Minusinsk depression. In this region, a paragenetic relationship between bentonites, volcanic, volcano-sedimentary and coal-bearing strata has been established, and a special geological and genetic type of bentonites, associated with coal-bearing formations has been distinguished (Belousov et al., 2017; Belousov and Krupskaya,

2019). The geological structure of the Yuzhno-Minusinsk depression consists of volcanic, volcano-sedimentary, terrigenous and carboniferous sediments of Devonian and Carboniferous age. The coal-bearing strata of the Middle and Upper Carboniferous age contain large deposits of hard coal. Bentonites occur lower at the border between volcano-sedimentary and coal-bearing formations, represented by Early-Middle Carboniferous strata of the Sarskaya suite and are confined mainly to the Chernogorskaya and Izykhskaya basins (Fig. 1 a,b). In addition to the 10th Khutor deposit, the Karatigeyskoe, Solnechnoe and Karasukskoe bentonite deposits are confined to the same age range within the basin (Fig. 1a).

### 2.2. Geological structure of 10th Khutor deposit

The 10th Khutor deposit is located in the northwestern part of the Chernogorsky basin. The bentonite-bearing strata is confined to the lower part of the coal formation. The formation is composed of conglomerates, sandstones, siltstones, mudstones, limestones, carbonaceous rocks with seams and interlayers of hard coals and bentonites (Fig. 1b,c).

The Carboniferous tuffaceous-sandy-clayey bentonite-bearing formation consists of 5 benches containing layers of bentonite (Sabitov

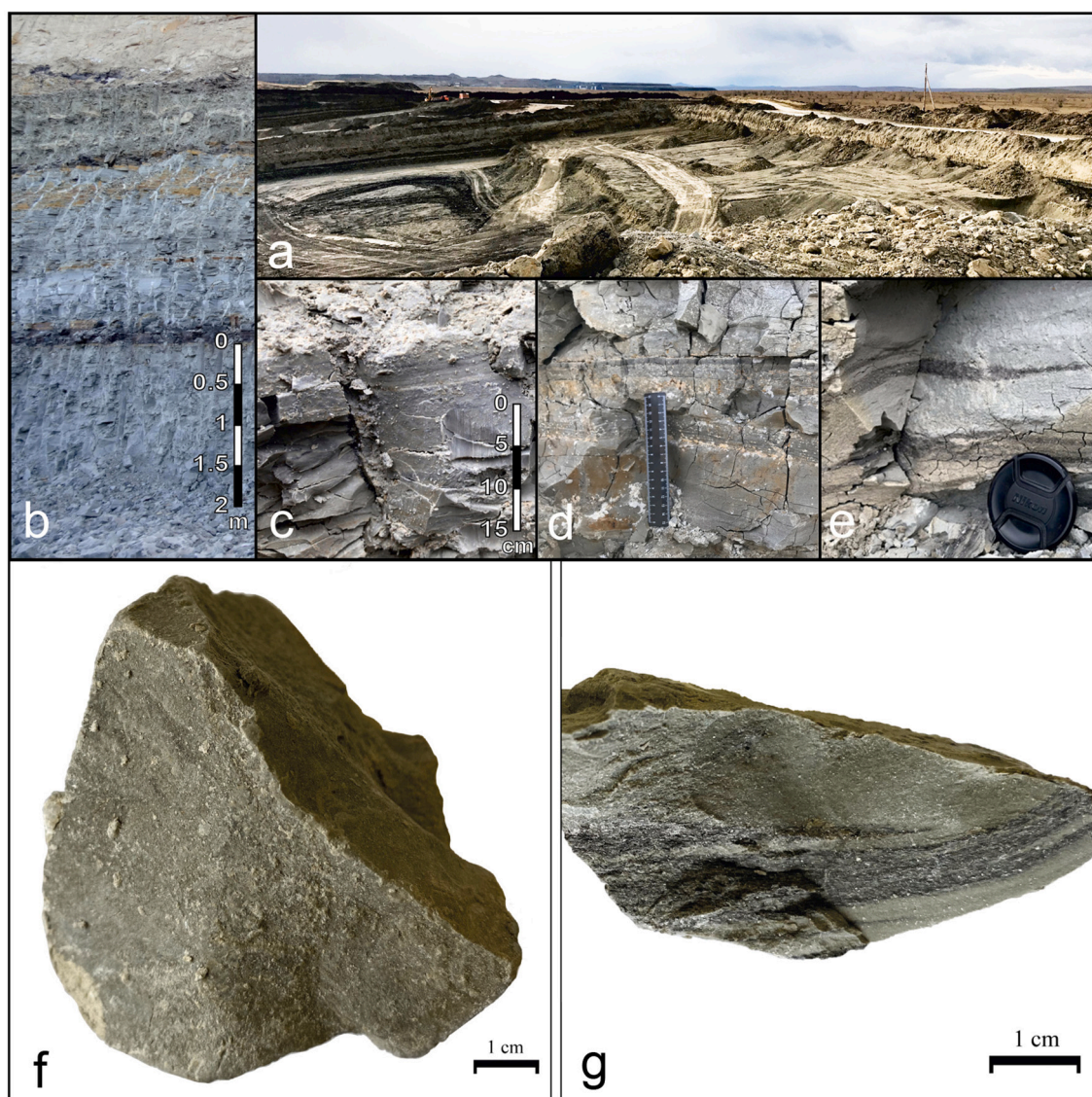


Fig. 2. Picture of the bentonite mine (a), bentonite layer IV (b) and representative samples with massive texture (c), interlayers (d), lenses of carbonaceous matter (e), sample 5A with a compacted texture (f) and sample 6E with laminated texture, containing microlayers of coalified matter (g).

et al., 2010). The second bench is of industrial importance, confined to Sarskaya suite ( $C_{1-2sr}$ ) of the Early-Middle Carboniferous strata, with a thickness of 35 m. This bench consists of 6 bentonite layers, interbedded with coal seams and tuff-terrigenous material (Fig. 1c). The IV, V and VI layers of bentonite are of greatest interest as they are used in various industrial applications and are characterized by the highest quality of raw materials. Higher in this section, there are the VII and VIII layers of bentonite, which are confined to the Chernogorskaya suite of the Middle Carboniferous ( $C_{2cr}$ ) and separated from the main bench by a 20-m layer of sandstones. The quality of the raw materials in layers VII and VIII is lower than in layers IV, V and VI and so they are not considered in this work. Bentonite layer III is not represented in the area of the deposit. The cut-off content of smectite for the industrial products, which has passed averaging after extraction and processing, is at least 60%.

Bentonite layers have monoclinic bedding with a northeastern course and dip to the southeast at an angle of 6–8° (Fig. 1c, 2b), with a mean thickness from 1.5 to 4 m. The layers are separated by terrigenous and carbonaceous rocks. Thick coal seams with interlayers of tonsteins of kaolinite composition occur higher in the section at Chernogorskaya suite of the Middle Carboniferous ( $C_{2cr}$ ). The thickness of the hard coal is up to 12 m while the thickness of the tonsteins averages 0.2–4 cm.

### 3. Materials and methods

#### 3.1. Materials

The work is based on a series of field trips to the 10th Khutor deposit from 2014 to 2019. During this period, variability in mineral and chemical composition were studied in detail. In the present article, the results of studying the bulk samples from productive layers (bentonite layers #2, 4, 5, 6) and their corresponding fine fractions  $<1 \mu\text{m}$  are given. Samples were taken sequentially from productive strata across bedding. In sample code labeling, the numbers represent the number of the layer, whereas the letter in the name of the sample refers to the specific sample from within the layer given by the code. These letters follow an alphabetical order from the bottom to the top of the given layer. Detailed analytical studies for the samples from each layer were carried out for the samples of raw material and their fine fraction (XRD, SEM, DTA, XRF, FTIR, BET and CEC analysis).

An industrial sample from the 6th productive layer with a relatively high content of montmorillonite (72%) was added to the studied collection under the number “IB-6”.

A fine fraction  $<1 \mu\text{m}$  from the samples of every layer was separated and labeled as “ $<1 \mu$ ”. The fine fraction was obtained from a 3% aqueous suspension using an OS-6MTs laboratory centrifuge (Dastan, Kyrgyzstan), after centrifugation for 9.5 min at 1200 rpm from a depth of 4 cm.

#### 3.2. Methods

The mineral composition of bulk samples and clay fractions was determined by X-ray diffraction (XRD). X-ray diffraction patterns were obtained with an Ultima-IV X-ray diffractometer (Rigaku, Tokyo, Japan), using  $\text{CuK}\alpha$  radiation, semiconductor 1D detector D/Tex-Ultra, scan range 3–65°2 $\theta$ , scan speed 3°2 $\theta$ /min and scanning step—0.02°2 $\theta$ . The mineral composition was analyzed according to Moore and Reynolds Jr (1999) recommendations, the quantitative composition was estimated by the Rietveld method (Post and Bish, 1989) using the BGMN code (Profex software, Version 3.14.3, Doebelin and Kleeberg, 2015).

In order to detect any possible illite layers in smectite the clay fractions were saturated with 1 M KCl overnight and washed repeatedly with distilled water to remove excess salt. Subsequently, they were saturated with 1 M  $\text{CaCl}_2$  overnight and washed repeatedly with distilled water to remove excess salt, pipetted off on glass slides and allowed to dry in atmospheric conditions. After drying the clay fractions were solvated in ethylene glycol vapours at 60 °C overnight and examined

with XRD.

Chemical analysis was determined with X-ray fluorescence spectrometry (XRF) using an Axios mAX XRF spectrometer (PANalytical, Almelo, The Netherlands) on beads prepared by fusion with lithium borate at 1200 °C. The samples had been previously dried at 110 °C. The iron content was determined as total  $\text{Fe}_2\text{O}_3$ .

The microstructure of the samples was studied with scanning electron microscopy (SEM) using a LEO1450VP SEM (Carl Zeiss, Oberkochen, Germany). Samples for SEM were prepared in the form of individual particles and aggregates. The samples in powder form were deposited on a double-sided electrically conductive adhesive tape. Then the excess sample particles were removed with compressed air. As a result, a monolayer of individual particles and aggregates on an adhesive tape was obtained. The studied surface was coated with a 5–10 nm thick gold film, under vacuum, to avoid electrical charging of the sample during analysis.

The thermal behavior of the samples was analyzed with a synchronous thermal analyzer TGA/DSC 3+, (Mettler Toledo, Switzerland). Thermal analysis of the industrial sample was performed with an EXSTAR TG / DTA 7300 (SII) instrument. The samples were heated in corundum crucibles at a constant heating rate of 10 °C / min. The experiments on the TGA/DSC 3+ were carried out in an atmosphere of artificial air (80% nitrogen, 20% oxygen), at a flow rate of 100 ml / min. To remove gases due to EXSTAR TG / DTA 7300 measurements released during heating, the furnace space was continuously purged with dry air obtained by passing it through a column with silica gel at a volumetric air circulation rate of 100 ml / min. The decomposition and fitting of thermal curves was performed using Fityk 1.3.1. software (Wojdyr, 2010).

The IR spectra were obtained using a Perkin Elmer Spectrum One FTIR spectrometer equipped with an Indium Gallium Arsenide (InGaAs) detector and a KBr beam splitter. For each sample, 100 scans were recorded in the MIR region (4000–400  $\text{cm}^{-1}$ ) with a resolution of 4  $\text{cm}^{-1}$ . To obtain a KBr pellet, 1 mg of sample was dispersed in 400 mg of KBr and the resulting mixture was placed in a 20 mm pellet die and pressed for 20–25 min. The pellet was placed in a glass desiccant box with  $\text{CaCl}_2$  and heated in a furnace at 150 °C for at least 20 h. Spectra processing was performed using the OPUS 7.0 software package (Bruker Ltd.). Baseline correction was made in Interactive mode using the Straight-line method with one iteration.

The calculation of structural formulae of smectites was carried out per half formula unit with a constant number of anions –  $\text{O}_{10}(\text{OH})_2$  and 2 octahedral cations based on the data of the XRF sample chemical composition, taking into account the impurities identified by X-ray diffraction determined by the Rietveld approach described above, and IR spectroscopy data. The ratio of  $\text{Fe}^{2+}/\text{Fe}^{3+} = 0.2$  in octahedral sheets of montmorillonite was obtained by the Mössbauer spectroscopy data. Mössbauer spectra were obtained at room temperature on a CM120 Mössbauer spectrometer (Russia). The instrumental linewidth in the spectrum of the reference  $\alpha\text{-Fe}$  was  $0.23 \pm 0.01 \text{ mm/s}$ . The angle between the normal to the generatrix of the cone and the direction to the source of gamma radiation was 54.7° in the Mössbauer spectrometer and made it possible to exclude the asymmetry of the quadrupole splitting doublets associated with the orientation of the sample (Ericsson and Wäppling, 1976). The density of the absorber for natural iron did not exceed 5  $\text{mg/cm}^2$ . The quality of the spectrum decomposition was assessed using the Pearson test ( $\chi^2$ ).

The specific surface area (SSA) was determined with a Quadrasorb SI/Kr analyzer (Quantachrome Instruments, Boynton Beach, FL, USA). Adsorption was performed at the temperature of liquid nitrogen (77.35 K). Nitrogen with a purity of 99.999% served as an adsorbate. Helium grade 6.0 (99.9999%) was used for the volume calibration of the measuring cells. The calculation was carried out by the BET multiple-point isotherm in the range of P/P0 from 0.05 to 0.30. Before measuring the surface characteristics, the samples were vacuum-pumped using the Flo-Vac Degasser installation, which is an integral

part of the Quadrasorb SI/Kr analyzer and allows pumping of gases and water from the pore space in the temperature range of 15–400 °C and control of the pressure in the system (with the sample) in the range of 101.3 kPa–0.133 Pa. In our work, the pumping of the samples was carried out at 100 °C (temperature of dehydration) to a residual constant

pressure in the system of 0.133 Pa. Using of a higher temperature can damage the structure of the aluminosilicates and, therefore, change the state of the pore space. The pumping time at this temperature was 4 h. The Density Functional Theory (DFT) method was used to calculate the volume and average pore size, and the T-method Halsey was used to

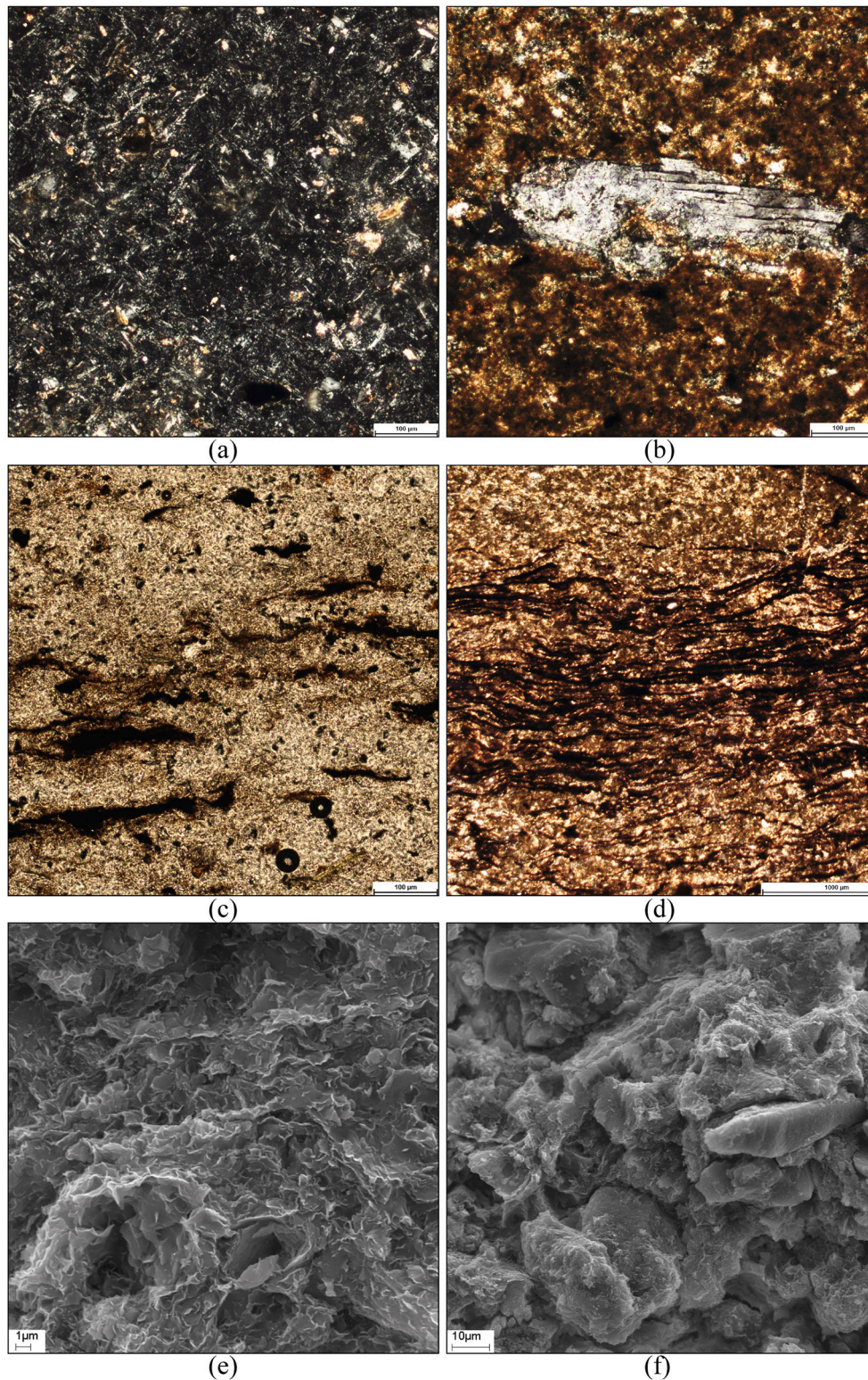


**Fig. 3.** Optical microphotographs and SEM pictures of bentonite samples: a, b – sample 5B, polished thin sections of bentonite with pelitic structure with inclusions of feldspar grain; c, d - sample 2B, polished thin sections of bentonite with layered structure and interlayers of carbonized organic matter; e - sample 5B, smectite in the form of flat and wavy flakes; f – sample 5B, smectite flakes covering the surface of detrital grains.

calculate the micropore volume and surface area of the micropore powder.

Determination of CEC was carried out by two methods (Belousov et al., 2020), by adsorption of methylene blue (MB) (Kaufhold et al., 2002) and Cu(trien) (Lorenz et al., 1999., Dohrmann et al., 2012). Adsorption of methylene blue gives an approximation rather than the real CEC value of the samples and was based on titration. The bentonite samples with distilled water (0.3 g/25 cm<sup>3</sup>) were preliminarily boiled in a water bath and treated with 1cm<sup>3</sup> sulfuric acid. Adsorption of Cu(trien) was performed as follows: the bentonite suspension (100 mg/50 cm<sup>3</sup>) was mixed with 10 ml of 0.01 M Cu(II)-triethylenetetraamine solution. The resulting centrifuged (3 min, 12,000 rpm) and photometric measurements were taken at 615 nm (Expert-003, Econix-Expert, Russia).

The composition of exchangeable cations was determined according to a modified method (Pokidko, 2019) using Pfeffer's reagent - a 0.1 M solution of NH<sub>4</sub>Cl in 70% ethyl alcohol (Molodtsov and Ignatova, 1975). Following Dohrmann et al. (2012), the 0.15 M solution of NH<sub>4</sub>Cl in 80 wt% ethyl alcohol was used to reduce the solubility of carbonates. Sequential six-fold processing was carried out using this solution. Then the solvent with displaced cations was distilled off from the collected volume, after which the precipitate was heat treated to decompose ammonium chloride, and then dissolved in a weakly acidic solution. The concentrations of exchangeable cations were determined by optical emission using a ContraA 300 atomic-absorption spectrometer (Analytik Jena, Germany).

Technological properties for the chapter 4.3.3 were determined on industrial samples of bentonite powders. Activation with soda ash was carried out using an industrial extruder with further aging for 1 month. Studies of rheological properties were determined in accordance with API Specification 13A on a rotational viscometer Fann Model 35. Casting properties were determined at Bentonite Khakassia LLC in accordance with GOST 28177–89 standard "Bentonite molding clays", 1989.

## 4. Results and discussion

### 4.1. Analytical research

#### 4.1.1. Structural features of the deposits

The bentonites from the 10th Khutor deposit contain interlayers of coal or coalified beds 0.1–1 m thick, confined either in the bottom or the top of the bentonite layers (Fig. 2b,d,e). In addition to coals, there are also small lenses and nodules of limestones, calcareous siltstones, sideritized siltstones, and fine-grained sandstones 5–20 cm thick (Fig. 2b).

Bentonites are mostly gray, dark gray, less often greenish or bluish gray with a massive texture (Fig. 2f, g), less often with schistosity. There are samples with microlayers of coalified matter (Fig. 2g). The study of polished thin sections showed that most samples have mainly pelitic or silty-pelitic structure with inclusions of individual mineral grains up to 0.7 mm (Fig. 3a, b). Some sectors of the deposit as well as individual samples display a phytotelitic, layered structure, in which lenses and interlayers of carbonized organic matter occur in the main clay mass (Fig. 3c, d). The organic matter might have formed in the coal-bearing layers and then, during fusinization of the organic matter, it was squeezed out into the ash mass in the form of an amorphous gel.

Smectite occurs in the form of flat and wavy flakes 0.5–3 μm in size (Fig. 3e). These flakes form larger aggregates and completely cover the surface of mineral grains (e.g. quartz, feldspars, etc) (Fig. 3f).

#### 4.1.2. Mineralogical composition

Bentonites of the 10th Khutor deposit consist predominantly of smectite with admixtures of kaolinite, chlorite, illite, quartz, feldspars, calcite and gypsum (Table 1).

The maximum smectite content was recorded in the IV, V and VI layers and reached a maximum of 70–72 wt% with an average content of 63 wt% (Table 1, fig. 54a). In addition to smectite, all beds contain kaolinite (0.7–6.8%), illite (2–5.3%) and chlorite (0.1–6.2%). Quartz,

**Table 1** Mineral composition of the examined samples, determined by Rietveld approach (wt%).

Sample	Layer	Smectite	Kaolinite	Illite	Chlorite	Quartz	Microcline	Albite	Gypsum	Calcite	Siderite	Ankerite	Goethite	Anatase	Hematite
2A	II	41.7	1	5	2.5	28.3	10.3	8.9	0.6	0.9	0	0	0	0.5	0.3
2B	II	30.4	1.2	5	2.1	37.7	11.5	9.6	0.4	1.4	0	0	0	0.5	0.2
2C	II	65	2.9	3.7	1.4	9.8	5.5	5.7	0.4	4.6	0	0.4	0	0.5	0.1
<1 μ	II	91.7	0	1.2	1	3	0.5	0	0	2	0	0	0	0.6	0
4A	IV	66.6	1.5	5.2	1.3	12.9	5.1	5	0	1.4	0	0	0	0.7	0.3
<1 μ	IV	85.3	0	4.9	2	4	1	0	0	2	0	0	0	0.8	0
4B	IV	61.7	5.8	5.3	2.2	6.8	1.8	1.3	0	0	0.5	0	12.8	0.8	1
4C	IV	72	1	4.5	0.5	10.1	5.3	5.3	0	1.3	0	0	0	0	0
5A	V	58.8	2.1	4.7	0.1	12.6	6.9	7	2.8	3	0	1.4	0	0.4	0.2
5B	V	52.9	0.7	4.1	1.4	18.2	13.5	4.8	1.2	1.6	0	0.9	0	0.4	0.3
5C	V	63	3.3	3.6	0.3	13.6	6.3	7	0.3	1.3	0	0.8	0	0.4	0.1
<1 μ	V	90.6	1	2.4	1.5	2.4	0.7	0	0	1	0	0	0	0.4	0
5D	V	56.1	6.8	3.4	6.2	8.8	1.1	0	3.2	0	11.1	0.1	0	0.4	0
6A	VI	41.9	1.4	4.3	0.3	15.5	14.6	6.9	0	3.1	10.5	0.3	0	0.6	0.6
6B	VI	69.5	1.6	2.4	1.2	12.6	5.6	4.7	0.5	1.1	0	0	0	0.7	0.1
<1 μ	VI	93.5	0	1.7	0	2.1	0.5	0	0	1.5	0	0	0	0.7	0
6C	VI	62.9	1.1	3.5	1.2	11.4	9.9	6.1	0.2	1	1.7	0	0	0.7	0.3
6D	VI	66.6	1.4	3.6	1	11.1	6.2	5	0.2	3	0	1	0	0.6	0.3
6E	VI	68.3	1.1	2	1.3	14.1	6.6	4.5	0.5	0.9	0	0	0	0.6	0.1
IB-6	-	71.6	0.5	3.7	0.7	12.1	4.1	4.4	0	0.7	0.7	0.8	0	0.7	0
<1 μ	-	92.4	0.5	3.7	0.7	2	0	0	0	0	0	0	0	0.7	0

potassium feldspar and plagioclase are the most abundant non-clay minerals. Minor gypsum (0–3.2%), calcite (0–4.6%), ankerite (0–0.8%), anatase (0–0.8%) and hematite (average 0–0.6%, up to 3.2% in single samples) are present in all layers. The gypsum crystals in bentonite samples are large - up to 0.5 cm in diameter. Siderite (up to 10–11%) is present only in the top of the V and the bottom of the VI layer. Also, there are rare grains of jarosite (up to 3%) and rutile (up to 0.5%). The main accumulations of gypsum, hematite and jarosite are confined to the top or bottom of layers, while goethite (12.8 wt%) occurs only in layer IV.

#### 4.1.3. Smectite characterization

According to X-ray diffraction data smectite from the raw samples is of alkaline-earth type, as evidenced by the (001) diffraction peaks at 15.3 and 14.9 Å (Fig. 4a). The composition of the interlayer complex of the raw samples is dominated by calcium and magnesium cations, whereas the sodium is considerably less abundant (Table 2).

However, all samples of the fine fraction <1 µm are characterized by an interlayer distance of the basal reflection (001) about 12.5 (Fig. 4b), indicating an alkaline smectite with a predominance of sodium cations in the interlayer complex (Table 2). Thus, the natural bentonite contains two phases of smectite layers with different cationic compositions detected by XRD and confirmed by the results of the analysis of the composition of interlayer cations. The apparent controversy between the interlayer composition of the bulk sample and that of the <1 µm fraction is explained considering that the bulk bentonite, which is dominated by Ca-rich smectite was compacted during diagenesis and flocculated and during dispersion was only partly disaggregated. As expected, flocculation was more pronounced in the Ca-rich smectite layers. Therefore, the flocculated preferentially Ca-smectite layers settled, yielding a suspension which contained preferentially Na-layers. This explanation is in agreement with the observed differences in the SSA (see below). The fine fractions of bentonite (sample < 1 µm) predominantly consisted of 85.3–93.5% smectite. Impurities included traces of illite, quartz, chlorite, anatase and kaolinite and calcite (Table 1).

X-ray powder diffraction patterns (Fig. 4b) of the studied bentonites are characterized by the main phase - smectite with a set of well-resolved characteristic *hk0* reflections and 4.48 Å (100), 2.56 Å (110), 1.696 (210). The smectite is dioctahedral, as was indicated by the (060) reflection with *d* = 1.499 Å.

Additional studies of the samples after K-saturation and subsequent back-Ca-saturation and EG-solvation, showed that the 001 peak of the EG-solvated samples after K-saturation and subsequent back Ca-saturation was slightly broader and the background at the low angle

**Table 2**

Composition of exchangeable cations, meq/100 g.

Sample	Total	Na <sup>+</sup>	K <sup>+</sup>	Ca <sup>2+</sup>	Mg <sup>2+</sup>
2C	65.6	26.6	1.7	15.1	22.3
2C <1 µ	93.4	56.4	3.5	16.3	17.2
4A	53.2	18.4	1.9	21.8	11.1
4A <1 µ	98	61	5.9	17.1	13.9
5C	58.8	14.2	2.6	21.6	20.3
5C <1 µ	90.2	47.6	3.2	17.5	21.8
6B	72.3	16.6	2	33.5	20.2
6B <1 µ	88.8	54.4	3.1	15.1	16.2
IB-6	76.3	19.3	2.7	40.9	13.4
IB-6 < 1 µ	104.1	74.9	4.7	10.6	14

side of the peak was higher than those of the original samples (Fig. 4c) which might indicate the presence of a small number of illite layers (<10%), i.e. limited illitization.

Thermal analysis provided information on some of the structural features of smectites, which affect the physicochemical properties of bentonites. As is typical for all smectites, two main endothermic effects are observed on the thermal curves (Fig. 5a). The first thermal effect at 80–194 °C is associated with the dehydration due to removal of adsorbed and interlayer water, with 11% mass loss (Reka et al., 2014) The dehydration peak at 152 °C confirms the presence of alkaline-earth cations in the interlayer space of natural bentonites (Fontaine et al., 2020). The second endothermic effect is associated with the loss of structural water from smectite with a mass loss of 4.9%. The dehydroxylation temperature at 667 °C indicates the predominance of cis-vacant octahedra (Drits et al., 1995). The prevalence of cis-vacant octahedra reflects the high heat resistance of the bentonite - one of the industrial quality indicators of raw materials, especially valuable for the use of bentonites in the foundry industry. The endothermic effect at 896 °C is a result of the collapse of montmorillonite structure. The total loss on ignition up to 1060 °C was 16.8% of the initial mass.

The dehydroxylation endothermic peak is asymmetric with a flat left shoulder; therefore, it was decided to decompose the peak. The endothermic event consists of a main peak, with a maximum at 664 °C, and a small endothermic event with a lower dehydroxylation temperature at 623 °C, which indicates structural heterogeneity of smectite (Fig. 5a). The presence of the weak dehydroxylation component at 505 °C might be associated with the kaolinite and siderite admixtures, the possible presence of a small fraction of illite layers or with the presence of a trans-vacant octahedral smectite (Drits et al., 1998). The weight loss of 1.2% at this temperature significantly exceeds the weight loss expected due to the kaolinite and siderite contents and illite interlayers in the industrial

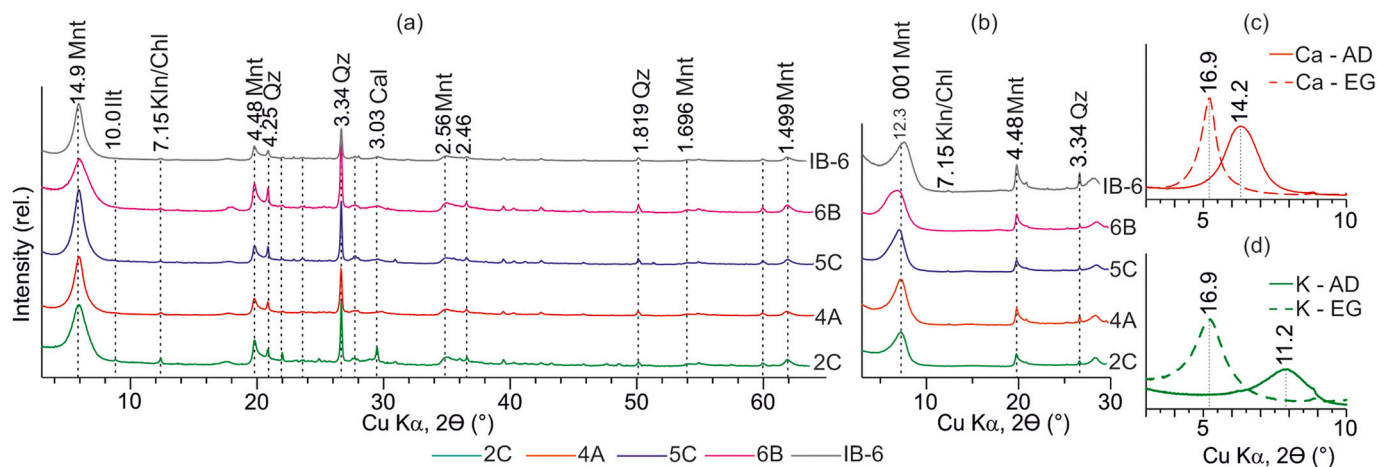


**Fig. 4.** X-ray diffraction traces of the samples from the 10th Khutor deposit: a – raw bentonite samples; b – bentonite fractures <1 µm; c – the sample IB-6 of air-dried (AD) and ethylene glycol solvated (EG) states; d – the sample IB-6 after K-saturation and subsequent back-Ca-saturation. Mt. – montmorillonite; I – illite; Kaol – kaolinite; Chl – chlorite; Q – quartz; Fsp – feldspars; Cal – calcite; Gp – gypsum.

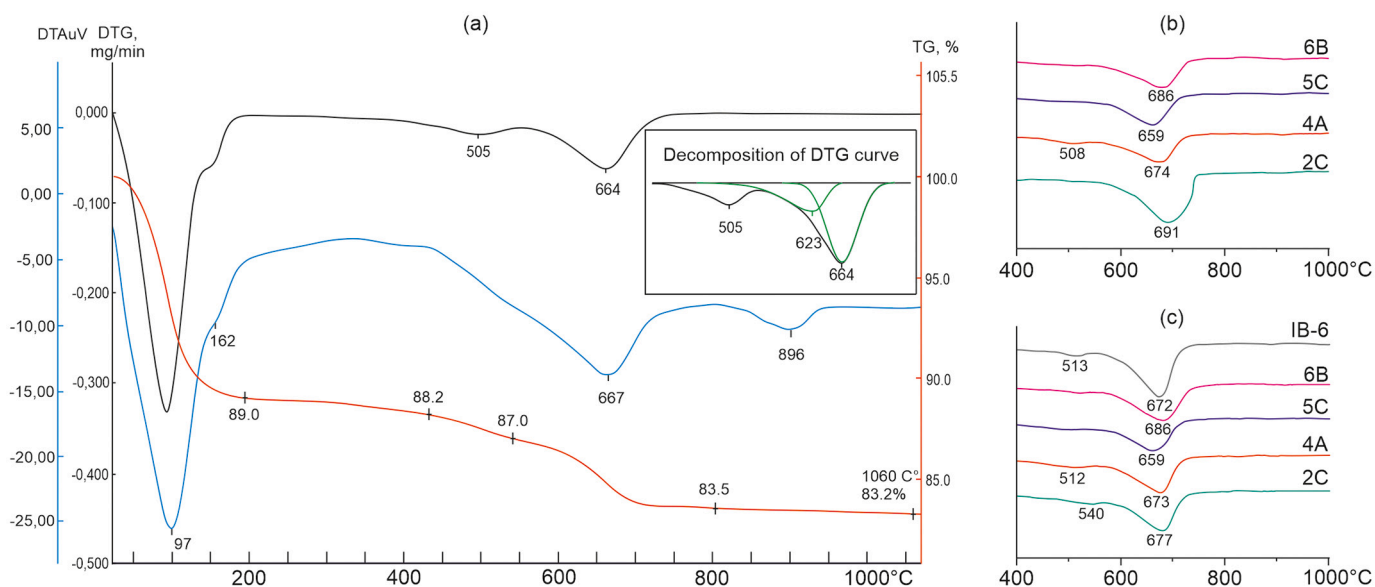


Fig. 5. TG and DTG curves of the industrial bentonite sample IB-6 (a), raw bentonite samples (b) and bentonite fractions <1 μm (c) from different layers.

sample IB-6 (Table 1). It is suggested that this endothermic event might also indicate the presence of low-temperature variety of smectite. It is suggested that these differences in the dehydroxylation temperature of montmorillonite are associated with the conditions of formation, which will be described in more detail below.

The thermal characteristics of natural bulk samples (Fig. 5b) and their <1 μm clay fractions (Fig. 5c) from each layer are consistent with the industrial sample IB-6. The dehydroxylation temperature of bulk

samples ranges from 662 to 695 °C, while the effect of fine fraction <1 μm ranges from 660 to 685 °C.

The FTIR spectroscopic study of <1 μm clay fractions from each layer confirm that they are mainly composed of dioctahedral smectite (Fig. 6). This is evidenced by the combination of the following characteristics of the IR spectra: the most intense band of Si–O stretching is relatively symmetrical and located at 1040 cm<sup>-1</sup>, with a doublet at 523 cm<sup>-1</sup> (Al–O–Si deformation) and at 466 cm<sup>-1</sup> (Si–O–Si deformation); the OH

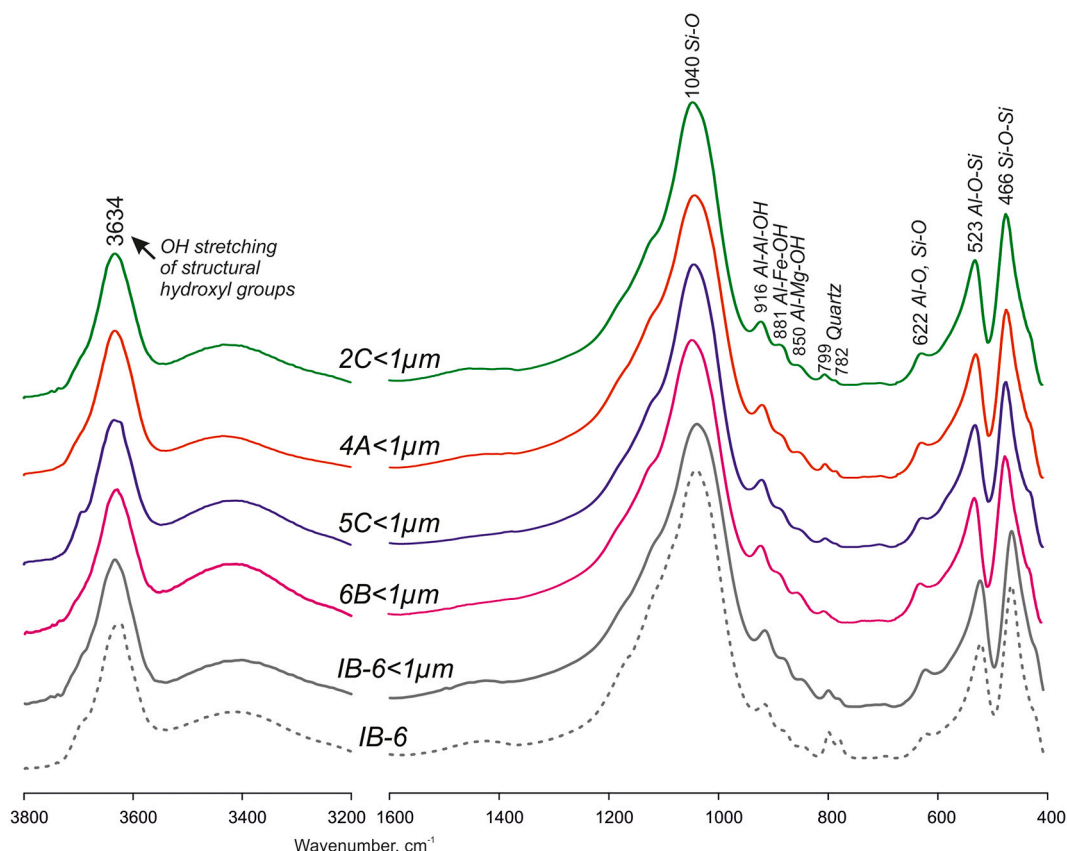


Fig. 6. IR spectra of the industrial bentonite sample IB-6 and bentonite fractions <1 μm from different layers.

stretching bands occur at  $3634\text{ cm}^{-1}$ . The absorption band near  $622\text{ cm}^{-1}$ , attributed to the coupled Al—O and Si—O out-of-plane vibrations, shows the high octahedral Al content, while the bands at  $881$  and  $850\text{ cm}^{-1}$  indicate octahedral substitutions of Fe for Al and Mg for Al, respectively (Farmer, 1974; Madejová and Komadel, 2005; Zviagina et al., 2004; Madejová et al., 2017). Therefore, all the studied clay fractions and industrial sample IB-6 have almost identical FTIR spectra in the MIR region and, accordingly, have a similar cationic composition of octahedral and tetrahedral sheets. The small shoulder at  $\sim 3690\text{ cm}^{-1}$  in the  $5\text{C}$   $<1\text{ }\mu\text{m}$  fraction and IB-6 samples indicate the presence of kaolinite, in accordance with the XRD analysis (Table 1).

The structural formulae were calculated for the clay fractions  $<1\text{ }\mu\text{m}$  from each layer (Table 3).

Since for geological conclusions it was important to characterize the composition of interlayer cations as close as possible to the original composition, homoionic forms were not prepared in this work. Using the detailed mineralogical characterization and accurate identification of impurities (Table 1), the following oxide abundances were subtracted from the chemical compositions (Table 4): for  $2\text{C}$   $<1\text{ }\mu\text{m}$  -  $\text{SiO}_2 = 4.10$ ,  $\text{Al}_2\text{O}_3 = 0.69$ ,  $\text{Fe}_2\text{O}_3, \text{FeO} = 0.46$ ,  $\text{MgO} = 0.14$ ,  $\text{CaO} = 1.08$ ,  $\text{K}_2\text{O} = 0.18$ ,  $\text{TiO}_2 = 0.60$ ;  $4\text{A}$   $<1\text{ }\mu\text{m}$  -  $\text{SiO}_2 = 7.43$ ,  $\text{Al}_2\text{O}_3 = 2.17$ ,  $\text{Fe}_2\text{O}_3, \text{FeO} = 1.03$ ,  $\text{MgO} = 0.28$ ,  $\text{CaO} = 1.10$ ,  $\text{K}_2\text{O} = 0.57$ ,  $\text{Na}_2\text{O} = 0.01$ ,  $\text{TiO}_2 = 0.80$ ;  $5\text{C}$   $<1\text{ }\mu\text{m}$  -  $\text{SiO}_2 = 4.77$ ,  $\text{Al}_2\text{O}_3 = 1.61$ ,  $\text{Fe}_2\text{O}_3, \text{FeO} = 0.72$ ,  $\text{MgO} = 0.18$ ,  $\text{CaO} = 0.55$ ,  $\text{K}_2\text{O} = 0.31$ ,  $\text{TiO}_2 = 0.40$ ;  $6\text{B}$   $<1\text{ }\mu\text{m}$  -  $\text{SiO}_2 = 3.26$ ,  $\text{Al}_2\text{O}_3 = 0.62$ ,  $\text{Fe}_2\text{O}_3, \text{FeO} = 0.07$ ,  $\text{MgO} = 0.06$ ,  $\text{CaO} = 0.81$ ,  $\text{K}_2\text{O} = 0.22$ ,  $\text{TiO}_2 = 0.70$ ;  $\text{IB-6}$   $<1\text{ }\mu\text{m}$  -  $\text{SiO}_2 = 4.19$ ,  $\text{Al}_2\text{O}_3 = 1.51$ ,  $\text{Fe}_2\text{O}_3, \text{FeO} = 0.44$ ,  $\text{MgO} = 0.12$ ,  $\text{CaO} = 0.02$ ,  $\text{K}_2\text{O} = 0.31$ ,  $\text{TiO}_2 = 0.70$ . After these corrections for impurities, the structural formulae determined are considered reliable.

The obtained structural formulae, in addition to the cationic composition, allowed estimation of the layer charge ( $0.44$ – $0.53\text{ mol.f.u.}$ ) and its distribution between tetrahedral ( $31$ – $38\%$ ) and octahedral ( $62$ – $69\%$ ) sheets. According to the classification proposed by (Emmerich et al., 2009), the smectite of all the samples is a high-charge beidellitic montmorillonites.

#### 4.1.4. Chemical composition

The average content of  $\text{SiO}_2$  and  $\text{Al}_2\text{O}_3$  in the bulk samples is  $60$  and  $15\%$  respectively, and in the  $<1\text{ }\mu\text{m}$  fraction it is  $58$  and  $21\%$  respectively (Table 4). This indicates a rather high content of Al in the structure of smectite. The increased content of calcium and iron oxide in raw samples are attributed to the presence of calcite, siderite and gypsum (Table 4).

The content of trace elements in general is typical for bentonites formed from acid volcanic ash (Kadir et al., 2019) (Table 5). This paper focuses on immobile elements such as Nb, Zr, Y, which are less mobile during alteration, which is mainly related to their low solubility in low-temperature aqueous solutions and may be more suitable for identifying the geochemical affinities of volcanic ash.

#### 4.1.5. Textural properties

The SSA of the bulk samples is  $26$  and  $28\text{ m}^2/\text{g}$  for the samples  $6\text{B}$  and  $2\text{C}$  respectively and  $43\text{ m}^2/\text{g}$  for the sample  $5\text{C}$ . At the same time, the SSA of the  $<1\text{ }\mu\text{m}$  clay fraction from the samples  $6\text{B}$  and  $5\text{C}$  is  $45$  and  $50\text{ m}^2/\text{g}$ , respectively.

The SSA of the industrial sample IB-6 is  $20\text{ m}^2/\text{g}$ . The low SSA values

of the industrial sample are most likely associated with the flocculation and compaction during diagenesis and their thermal treatment during the drying of raw materials at the plant, which led to particle agglomeration. The SSA of the  $<1\text{ }\mu\text{m}$  clay fraction from the industrial sample IB-6 is  $43\text{ m}^2/\text{g}$ . Also in all samples the SSA of the  $<1\text{ }\mu\text{m}$  clay fraction is higher than that of the original sample (Table 6). The higher SSA of the clay fraction most likely reflects the partial deflocculation of the materials mentioned before. An alternative possibility would be that, due to diagenesis, the smectite particles display partial 2D ordering similar to Wyoming smectites (Vantelon et al., 2018), which might lead to larger particles. This might lead to higher SSA. However, this possibility does not explain the different SSA values between the bulk clay and the  $<1\text{ }\mu\text{m}$  clay fraction by itself. In any case, more analytical work is necessary to support this possibility, which is beyond the scope of this study.

At the same time, the samples  $6\text{B}$  and  $2\text{C}$ , which have a low SSA, do not have microporosity, whereas the SSA of sample  $5\text{C}$  attributed to microporosity is only  $5\text{ m}^2/\text{g}$  i.e.  $\sim 10\%$  of its total SSA. The SSA of the fine fractions of the samples attributed to microporosity varies from  $4$  to  $19\text{ m}^2/\text{g}$ .

The lowered values of microporosity and of SSA in bulk samples might be associated with the conditions of bentonite formation, discussed in the next chapters.

#### 4.2. Genesis and conditions of formation

The main objective of this work was the study of the genesis and formation conditions of bentonites from the 10th Khutor deposit, which is of exceptionally old age. This issue was not addressed in detail previously and was open to speculation. The bentonite occurrence of this area is confined to the Minusinsk coal basin. The conditions of sedimentation of fossil coals are favorable for the formation of bentonites from pyroclastic material (Dai et al., 2017a, 2017b). The original tuff material has not been preserved along the deposit. The ratios of trace elements were used to establish some characteristics of the source rocks. Since most of the trace elements can migrate during diagenesis, the elements Ti, Nb, Zr, Y and Ta were used as the most immobile elements (Winchester and Floyd, 1977; Huff et al., 1993). Their ratio was used to restore the composition of the source rocks. The obtained results indicate rhyodacitic-dacitic composition of the initial ashes (Fig. 7).

Studies of the fraction, washed from the clay, made it possible to find fragments of a glass shard pseudomorphically replaced by smectite (Fig. 8a) and transformed feldspar grains (Fig. 8b).

Thermal analysis showed that there are cis-vacant octahedra in the studied smectite, as evidenced by the high temperature of the predominant second endothermic event (Fig. 5). The presence of trans-vacant positions is usually associated with illitization processes and indicates the presence of processes of continental weathering of primary micas and illite (Drits et al., 1995). However the bentonite does not display evidence of significant illitization and formation of abundant mixed-layer illite-smectite (Fig. 4b, c). The limited illitization might partially explain the low temperature endothermic event at  $\sim 505\text{ }^\circ\text{C}$  (Drits et al., 1998) (Fig. 5a). The weight loss due to this event requires the presence of a montmorillonite with lower dehydroxylation temperature.

The study of paleogeographic maps (Pozner, 1969) made it possible to reconstruct the sedimentary environment in the studied region. Such

**Table 3**  
Cation compositions and layer charge of the studied smectites (atoms per  $\text{O}_{10}(\text{OH})_2$ ).

Sample	Tetrahedral		Octahedral				Layer charge		
	$\text{Si}^{4+}$	$\text{Al}^{3+}$	$\text{Al}^{3+}$	$\text{Fe}^{3+}$	$\text{Fe}^{2+}$	$\text{Mg}^{2+}$	Tet.	Oct.	Total
$2\text{C}$ $<1\text{ }\mu$	3.81	0.19	1.46	0.21	0.00	0.33	-0.19	-0.32	-0.51
$4\text{A}$ $<1\text{ }\mu$	3.85	0.15	1.53	0.17	0.00	0.31	-0.15	-0.29	-0.44
$5\text{C}$ $<1\text{ }\mu$	3.83	0.17	1.54	0.18	0.01	0.28	-0.17	-0.28	-0.45
$6\text{B}$ $<1\text{ }\mu$	3.85	0.15	1.50	0.16	0.04	0.31	-0.15	-0.34	-0.49
$\text{IB-6}$ $<1\text{ }\mu$	3.83	0.17	1.46	0.16	0.04	0.34	-0.17	-0.36	-0.53

**Table 4**  
Chemical composition of rock-forming elements (wt%).

N <sup>o</sup>	LOI	Na <sub>2</sub> O	MgO	Al <sub>2</sub> O <sub>3</sub>	SiO <sub>2</sub>	K <sub>2</sub> O	CaO	TiO <sub>2</sub>	MnO	Fe <sub>2</sub> O <sub>3</sub>	P <sub>2</sub> O <sub>5</sub>	SO <sub>3</sub>
2A	9.74	1.22	1.75	12.63	61.07	1.75	0.77	0.55	0.081	10.10	0.11	0.13
2B	7.77	1.18	1.60	11.69	72.09	2.02	0.64	0.53	0.051	2.14	0.09	0.09
2C	15.55	1.04	2.85	16.87	54.49	1.00	3.58	0.54	0.034	3.56	0.24	0.12
<1 μ	8.51	2.42	3.46	20.32	57.54	0.77	1.59	0.64	0.022	4.46	0.05	<0.10
4A	14.02	0.89	2.71	16.32	58.25	1.36	1.43	0.78	0.01	3.80	0.20	0.20
<1 μ	7.46	1.69	3.43	21.06	58.69	0.92	1.56	0.84	0.006	4.01	0.13	<0.10
4B	15.90	1.00	2.95	17.26	56.83	0.99	0.73	0.81	0.01	3.25	0.10	0.14
5A	13.63	0.98	2.82	16.19	59.72	1.09	1.56	0.43	0.014	3.28	0.08	0.07
5B	15.46	1.07	2.64	14.89	58.49	1.24	1.86	0.42	0.015	3.17	0.09	0.16
5C	13.03	1.31	2.51	16.69	59.43	1.32	1.66	0.48	0.01	3.31	0.11	0.14
<1 μ	8.17	1.64	3.42	21.86	58.50	0.63	0.95	0.44	0.007	4.17	0.04	<0.10
6A	11.08	1.30	2.40	14.37	51.86	1.41	5.85	0.65	0.604	9.99	0.28	0.05
6B	15.67	0.98	2.97	16.00	57.86	0.88	1.21	0.71	0.010	3.29	0.11	0.11
<1 μ	8.02	1.91	3.65	20.81	58.92	0.58	1.35	0.70	0.011	3.78	0.10	<0.10
6C	5.38	1.24	2.85	18.27	64.27	1.26	1.63	0.77	0.056	3.88	0.20	0.06
6D	15.25	0.89	2.91	16.31	58.76	0.85	1.08	0.67	0.008	2.97	0.09	0.05
6E	14.89	0.87	2.78	15.78	59.77	0.89	1.10	0.65	0.011	2.93	0.11	0.06
IB-6	11.36	1.00	2.84	17.43	59.47	1.04	2.13	0.76	0.05	3.78	0.13	0.00
<1 μ	7.21	2.04	3.48	21.19	58.87	0.64	1.38	0.77	0.021	4.17	0.08	0.05

**Table 5**  
Chemical composition of trace elements, ppm.

N <sup>o</sup>	Cr	V	Co	Ni	Cu	Zn	Rb	Sr	Zr	Ba	U	Th	Y	Nb	Pb	As	Cl
2A	36	76	16	29	24	132	79	179	324	350	<5	19	40	18	47	13	237
2B	37	70	10	15	19	48	101	154	312	433	<5	16	34	16	28	<10	100
2C	14	30	<10	16	10	64	54	291	370	273	9	20	99	21	40	14	428
5A	11	31	<10	15	<10	98	60	230	397	325	6	20	68	22	45	<10	148
5B	19	33	<10	21	19	98	61	1868	367	351	<5	21	65	20	41	14	216
4A	13	32	10	12	<10	81	49	414	416	374	<5	21	75	25	33	<10	375
6A	21	61	<10	12	12	83	50	287	263	343	<5	11	47	15	39	<10	108
6B	<10	46	10	16	<10	90	44	248	356	220	<5	12	50	18	35	47	102
6C	13	54	<10	14	<10	87	53	295	347	306	<5	10	51	17	33	<10	85
6D	<10	43	11	13	<10	94	47	255	368	285	<5	13	47	17	26	<10	107
6E	<10	43	10	16	19	76	48	226	393	266	<5	15	49	14	51	<10	93

**Table 6**  
Textural properties of studied mineral sorbents.

Sample	Specific surface area S <sub>BET</sub> , m <sup>2</sup> /g	Pores volume, nm	Average diameter, nm	Microporosity (volume) (T-method Halsey), cm <sup>3</sup> /g	Specific surface area (T-method Halsey), m <sup>2</sup> /g		
					Micropores	Meso-macropores	Total
IB-6	20	0.069	6	0	0	20	20
IB-6 < 1 μ	43	0.089	3.8	0.010	4	39	43
6B	26	0.086	6	0	0	26	26
6B < 1 μ	45	0.008	6	0.0015	16	29	45
5C	43	0.087	3.8	0.006	5	38	43
5C < 1 μ	50	0.091	3.8	0.018	19	31	50
2C	28	0.086	6	0	0	28	28

maps do not reflect the real position of the continents, but are the result of displaying a paleogeographic situation of a certain age, superimposed on a modern geographical map.

The beginning of the formation of the Yuzhno-Minusinsk depression was associated with volcanogenic-sedimentary material. It was a fore-deep with the accumulation of sediments transported from the neighboring mountain structures. In the Middle Devonian, the territory underwent maritime transgression, with the formation of a relatively shallow marine area with the surrounding low-mountain structures, which were the source of the transportation of thin silty material. At the beginning of the Carboniferous period the volcanic activity began. During these active periods, the territory mainly accumulated coarse terrigenous and volcanoclastic material brought in by nearby rivers. The climate at this time was moderately humid. The beginning of the formation of coal- and bentonite-bearing formations coincided with the largest paleoecosystem restructuring. The beginning of the

accumulation of sediments of the Sarskaya suite was accompanied by the activation of the Western Sayan (Pozner, 1969).

One of the questions that arose was the determination of the type of reservoir where pyroclastic material was accumulated. The presence of admixtures of gypsum crystals up to 5 mm in diameter and carbonate rocks in all bentonite strata suggests that the reservoirs were represented by a shallow water zone with an inland sea, bays and lagoons characterized by intense evaporation. The Minusinsk basin was a shallow part of the shelf with the accumulation of plant material. The Altai uplift from the south and the Sayan Mountains from the west served as areas for the removal of terrigenous material (Fig. 9). In the Middle Carboniferous, there was a sudden warming event and an increase in diversity in the composition of plant communities, which caused the appearance of thick coal seams. Thus, the geological development of the Minusinsk basin, suggests that from the beginning of the Visean age, the basin was lagoon (Pozner, 1969).

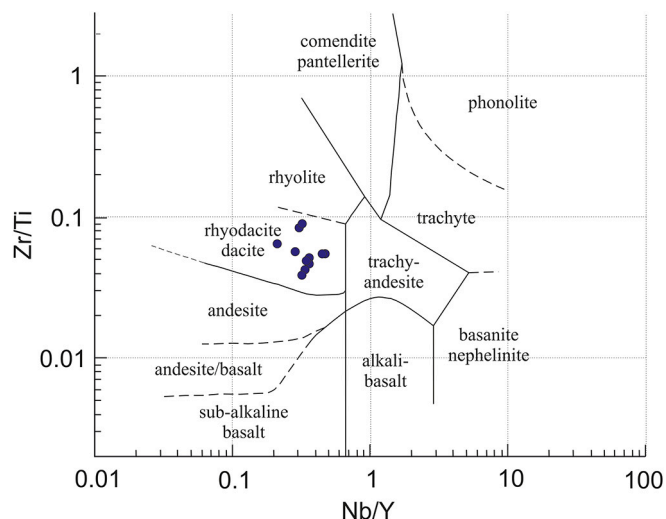


Fig. 7. Compositions of the 10th Khutor bentonites plotted in the diagram of Winchester and Floyd (1977).

However, higher in the section, in the coal deposits of the Chernogorskaya suite ( $C_{2cr}$ ), there are interlayers and lenses of tonsteins - clay formations of kaolin composition formed at lower pH values (Arbuzov, 2007; Arbuzov et al., 2019; Vergunov et al., 2020). Still the source of volcanogenic pyroclastics in the Minusinsk basin has not been identified with certainty. Bogomazov (1961) suggested that the centers of volcanic eruptions in the Early and Middle Carboniferous period were located in the west and northwest of the Altai-Sayan orogenic belt. In contrast Arbuzov et al. (2017) suggested that the source could be located in the south of the region, on the territory of modern Mongolia or Transbaikalia.

A distinctive feature of bentonite of the 10th Khutor is the fact, that despite the age of the deposit, which is about 350 million years, and the presence of deep burial diagenesis or even an initial phase of metamorphism, as evidenced by the formation of coal with laminated texture, these bentonites retained the ability to swell. Moreover, bentonites of such an ancient age are usually characterized by the formation of significant amount of a mixed-layer illite-smectite phase (Huff, 2016). However, the present study reveal the presence of a limited fraction of illite interlayers in the swelling component of bentonites, although mineralogical evidence indicates that there was potassium available in the system, because K-feldspar is present as minor phase in all samples

(Table 1). Dissolution of K-feldspar has been considered a main source of K for illitization of smectite during diagenesis (Hower et al., 1976). This was not observed in the present study because K-feldspar was preserved. Thus, it can be argued that the main component of bentonites from the 10th Khutor deposit is actually montmorillonite. The reasons for which K-feldspar preserved during diagenesis are not clear.

It is suggested that the alteration of the ashes took place in lagoonal environment under intensive evaporation conditions, as it is indicated by the presence of large gypsum crystals. Such an environment is characterized by high salinity and alkalinity which would ensure the presence of abundant potassium in pore waters. The high concentrations of soluble salts in the pore waters might have caused flocculation of the smectite particles leading to the compaction of the formation and causing the observed low microporosity and decreasing permeability. This in turn would have hindered potassium diffusion and retarded illitization. An alternative possibility would be that, due to diagenesis, the smectite particles display partial 2D ordering similar to Wyoming smectites (Vantelon et al., 2018), which might lead to larger particles. However, more analytical work is necessary to support this possibility, which is beyond the scope of this study.

#### 4.3. Industrial application and properties

##### 4.3.1. General properties

The geological conditions of the formation of bentonites of the 10th Khutor deposit affected their properties. After the diagenetic stage, the already formed bentonites were affected by the deep burial diagenesis or even initial stage of metamorphism, as evidenced by the seams of hard coal. In accordance with the coalification, the pressure of the overlying rocks for long-flame coals was 39.2–66.2 MPa (Mironov, 1991; Shestakova, 2010). The moisture content of the raw material is 21–25% (Table 7), which is low for diagenetic bentonites.

##### 4.3.2. Cation exchange capacity

The CEC determined by MB ranges from 23 to 27  $\text{cmol} \cdot \text{kg}^{-1}$  for samples from layer II and 54–63  $\text{cmol} \cdot \text{kg}^{-1}$  for samples from layers IV, V and VI (Fig. 10). The CEC determined for the purified fraction (sample  $< 1 \mu\text{m}$ ) is 89  $\text{cmol} \cdot \text{kg}^{-1}$ . The CEC values determined with the Cu (trien) complex were higher, namely 31–35  $\text{cmol} \cdot \text{kg}^{-1}$  for layer II and 50–80  $\text{cmol} \cdot \text{kg}^{-1}$  for samples for layers IV, V and VI. Also, the CEC of the  $< 0.5 \mu\text{m}$  fraction determined with the Cu (trien) complex was 102  $\text{cmol} \cdot \text{kg}^{-1}$ . A strong correlation between the CEC value and the MMT content along with a rather high coefficient of determination, both for MB and copper complex, indicates that montmorillonite was the only

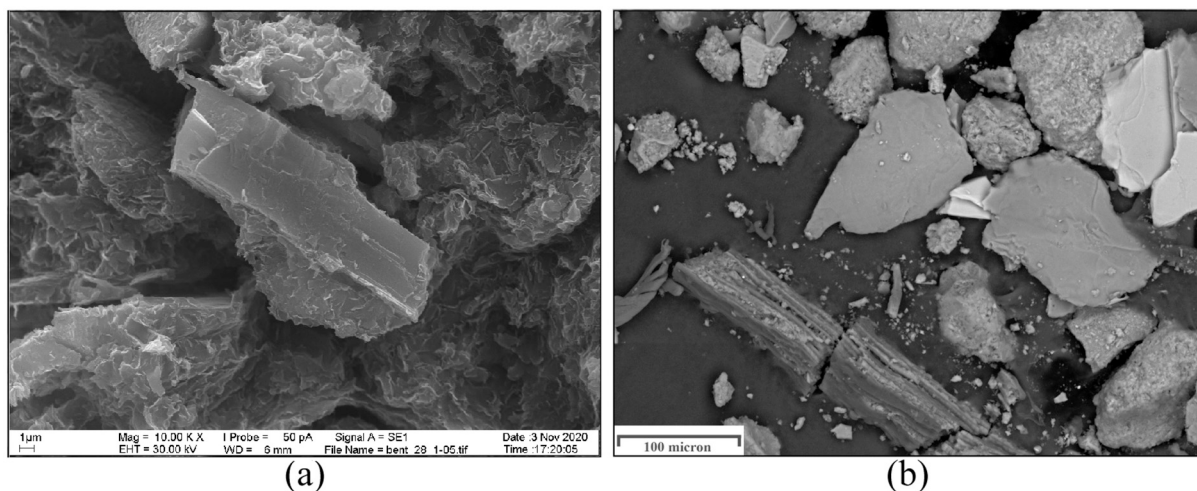
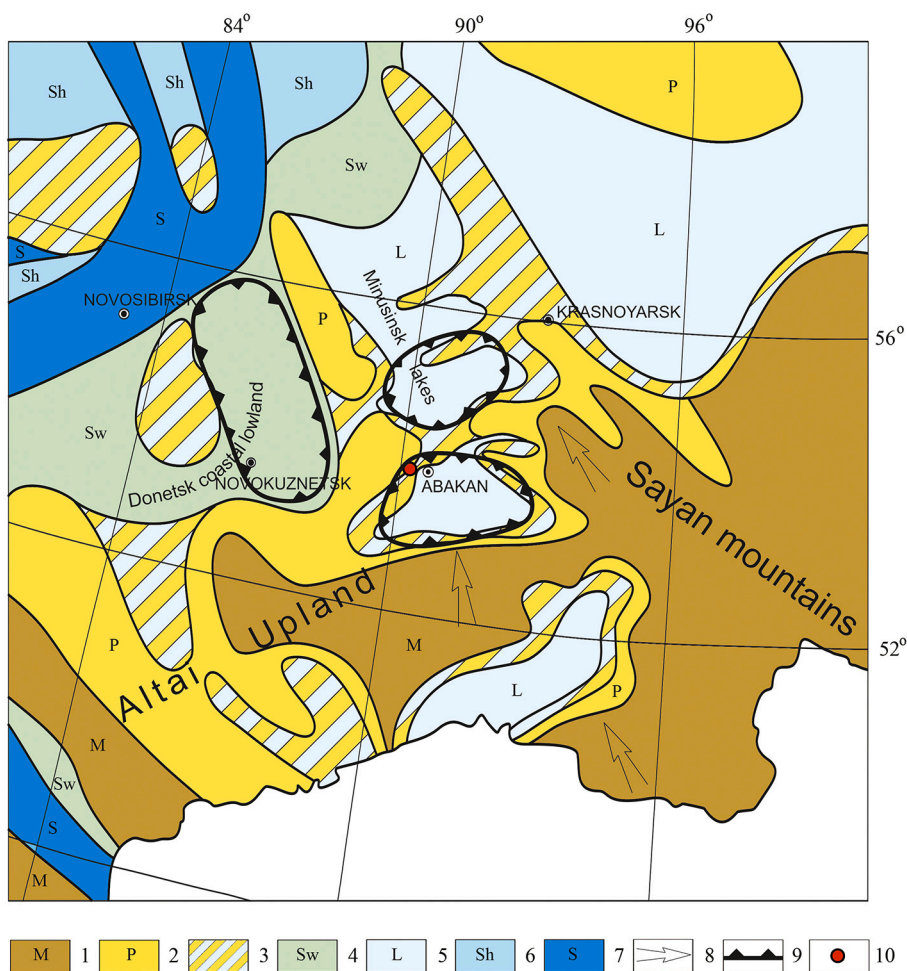


Fig. 8. Optical microphotographs and SEM pictures of washed crystalline impurities from 10th Khutor deposit, sample 5B: a – pseudomorphic alteration of volcanic glass shards; b - transformed feldspar grains.



**Fig. 9.** Lithological-paleogeographic scheme. Early-Middle Carboniferous system. (Pozner, 1969 with additions and revision). Legend: 1 - mountain land; 2 - inland plains; 3 - coastal plains, at times flooded by the sea; 4 - freshwater lakes and swamps; 5 - shallow water zone with an inland sea, bays and lagoons; 6 - shallow part of the shelf; 7 - sea and deep part of the shelf; 8 - direction of transportation of debris; 9 - zones of coal accumulation; 10 - 10th Khutor deposit.

**Table 7**  
Industrial properties of the sample IB-6 from the 10th Khutor deposit.

Condition of the bentonite	Basic		Rheological			Foundry	
	Raw-state moisture, %	Swelling index, ml/2 g	F600*	YP/PV**	Filtrate volume, ml	Green Compression Strength, N/sm <sup>2</sup>	Wet Tensile Strength, N/sm <sup>2</sup>
Natural	21–25	4	<4	–	–	4.9	0.14
Soda ash activation		27	34	5.6	12	10.7	0.30

\* Viscometer Dial Reading at 600 rpm.

\*\* Yield Point/Plastic Viscosity Ratio.

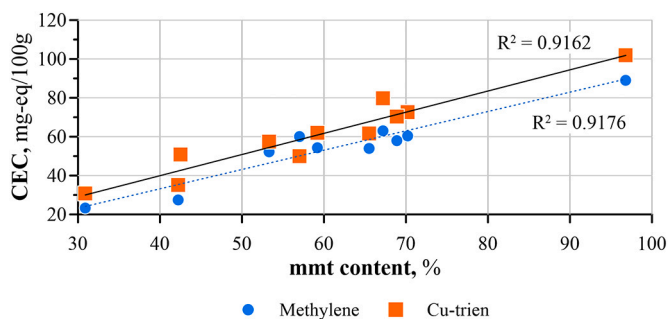


**Fig. 10.** Correlation of the CEC values with the montmorillonite content (wt%).

mineral affecting the CEC values (Fig. 10).

As was shown in previous works (Bujda'k and Komadel, 1997; Belousov et al., 2020), such a large difference in CEC values obtained by different methods may be attributed to the fact that in the presence of doubly charged cations in the interlayer space, the adsorption of the MB dye decreases. At the same time, the method for determining CEC by adsorption of Cu-trien is distinguished by a high ability to replace divalent metal cations in the interlayer space of montmorillonite due to the high selectivity of the basal surfaces of smectite for the copper complex.

Another reason for the observed difference for the measured CEC values by the adsorption method of MB and Cu-trien in bentonites of the 10th Khutor deposit is a low microporosity, which causes incomplete dispersion of the smectite particles and reduces the adsorption of MB on the surface of the smectite particles. Thus, it can be concluded that in the

case of the 10th Khutor deposit, the method with Cu-trien adsorption gives more accurate results for the CEC.

#### 4.3.3. Industrial properties

As mentioned above, bentonites from the 10th Khutor deposit are the main materials used by Russian IOP and foundries. This is due to the thermal stability of these raw materials along with their strength characteristics. The testing of technological samples indicates the high quality of sand-clay specimens based on this bentonite (Table 7). However, to achieve such quality characteristics, it is necessary to carry out mechanical activation and aging of the bentonite after the addition of soda ash. The studies were carried out on the industrial sample IB-6 in its original state, as well as after activation with soda ash. The Green Compression Strength of sand molding in its natural state is 4.9 N/cm<sup>2</sup>; while after activation with soda ash, it is 10.7 N/cm<sup>2</sup>. The Wet Tensile Strength of sand molding before and after activation is 0.14 and 0.30 N/cm<sup>2</sup>, respectively.

The swelling index of the original bentonite is 4 ml/2 g, which after activation with soda ash increases to 27 ml/2 g (Table 7). The rheological properties of bentonite also develop only after activation. A viscometer dial reading at 600 rpm is 34 (17 cpoise) and the Yield point to Plastic viscosity ratio is 5.6. Despite the formal compliance of the parameters of activated bentonite for the production of OCMA grade fluids according to API 13A specification (API 13 A, 2006, only bentonite powders of lower grades B and C (according to the Russian classification) are produced on the basis of this bentonite.

In connection with the emergence of a large Russian project for the construction of deep disposal sites for radioactive waste in the crystalline massif at depths of 550–750 m in Yeniseyskiy site (Dorofeev et al., 2017a, 2017b; Krupskaya et al., 2018, 2020; Abramov et al., 2020), as well as the beginning of laboratory and field experiments on the stability of engineered barrier systems, this bentonite is considered as a potential raw material.

## 5. Conclusion

The 10th Khutor bentonite deposit, located in the Republic of Khakassia (Russia) provides bentonite products for most foundries, ore mining and processing plants. The deposit is located within the development of continental tuff-sandy-argillaceous formation of the Chernogorsky basin which is confined to the Early-Middle Carboniferous sediments of the Sarskaya suite (C<sub>1-2sr</sub>). The bench consists of 6 layers of bentonite, interbedded with coal seams and tuff-terrigeneous material. The content of montmorillonite range from layer IV to VI and reaches a maximum of 69–72%, with an average content of 55 to 70%. The main impurities are quartz, K-feldspar, albite and siderite. Kaolinite, illite, chlorite, gypsum, calcite and ankerite are minor impurities.

The structural formulae of the smectite present is characterized as high-charged beidellitic montmorillonite. The high dehydroxylation temperature indicates the predominance of cis-vacant octahedra. The trace element composition of bentonites, as well as the presence of relics of volcanic glass and feldspar with a porous and layered structure, indicate that these bentonites are diagenetic. Based on the Nb/Y and Zr/Ti ratios the composition of the parent material was probably rhyodacitic-dacitic.

The paleogeographic maps and mineralogical composition suggest that the accumulation of parent tuff took place in lagoons. The influence of deep burial diagenesis or even initial stage of metamorphism, as evidenced by seams and packs of hard coal with laminated texture, affected the textural and surface properties of bentonites.

In the evaporitic depositional environment the high concentrations of soluble salts in the pore waters might have caused flocculation of the smectite particles leading to the compaction of the formation and causing the observed low microporosity and decreasing permeability. This in turn would have hindered potassium diffusion and retarded illitization, which remained limited. An alternative possibility would be

that, due to diagenesis, the smectite particles display partial 2D ordering, which might lead to larger particles. However, more analytical work is necessary to support this possibility, which is beyond the scope of this study.

Activation with soda ash significantly improved the swelling properties and strength of the bentonite. Testing of technological samples confirmed the high quality of sandy-clay forms based on this bentonite.

## Funding and Acknowledgments

This work was financially supported by the Russian Science Foundation (project No. 16-17-10270). Crystal chemical formulation as well as CEC estimation were carry out with the financial support of Russian Foundation for Basic Research (project No. 18-29-12115).

Experimental studies were partially performed using the equipment acquired with the funding of Moscow State University Development Program (X-ray Diffractometer Ultima-IV, Rigaku and Scanning Electron Microscope LEO 1450VP, Carl Zeiss).

The authors are grateful to A. Yakushev, N. Karelina (IGEM RAS), S. Garanina (MSU) and B. Pokidko (MIREA) for their help in carrying out the study. The authors also express their gratitude to the “Bentonite Company” and “Bentonite of Khakassia” companies for the provided materials and the opportunity to conduct field work at the 10th Khutor deposit.

## Credit author statement

We thank you for the time and effort spent in reviewing our manuscript. Based on your comments we have corrected some figures of the new version.

## Declaration of Competing Interest

None.

## References

- Abramov, A.A., Bolshov, L.A., Dorofeev, A.N., Igin, I.M., Kazakov, K.S., Krasilnikov, V. Y., Linge, I.I., Trokhov, N.N., Utkin, S.S., 2020. Underground research laboratory in the Nizhnekanskiy Massif: evolutionary design study. *Radioact. Waste* 1 (10), 9–21. <https://doi.org/10.25283/2587-9707-2020-1-9-21>.
- Alther, G.R., 1991. Thermal stability of some industrial bentonites. *Appl. Clay Sci.* 5, 469–488.
- American Petroleum Institute (API) Specification 13A, 2006. Specification for Drilling Fluid Materials.
- Arbuzov, S.I., 2007. Metal-bearing of siberian coals. *Bull. Tomsk Polytechnic Univer.* 311 (1), 79–84.
- Arbuzov, S.I., Ilyenok, S.S., Vergunov, A.V., Shaldybin, M.V., Sobolenko, V.M., Nekrasov, P.E., 2017. Mineralogical and geochemical identification of the products of the explosive volcanism in the coals of the Minusinsk basin. In: *Materials of the Conference Petrology of Magmatic and Metamorphic Complexes*, pp. 35–37. In Russian.
- Arbuzov, S.I., Spears, D.A., Vergunova, A.V., Ilenoka, S.S., Mezhibora, A.M., Ivanova, V. P., Zarubina, N.A., 2019. Geochemistry, mineralogy and genesis of rare metal (Nb-Ta-Zr-Hf-Y-REE- Ga) coals of the seam XI in the south of Kuznetsk Basin, Russia. *Ore Geol. Rev.* 113, 103073.
- Belousov, P.E., Krupskaya, V.V., 2019. Bentonite clays of Russia and neighboring countries. *Georesursy* 21 (3), 79–90. <https://doi.org/10.18599/grs.2019.3.79-90>.
- Belousov, P.E., Krupskaya, V.V., Zakusin, S.V., Zhigarev, V.V., 2017. Bentonite clays from 10<sup>th</sup> Khutor deposit: features of genesis, composition and adsorption properties. *RUDN J. Eng. Res.* 18 (1), 135–143 (in Russ.). [10.22363/2312-8143-2017-18-1-135-143](https://doi.org/10.22363/2312-8143-2017-18-1-135-143).
- Belousov, P.E., Pokidko, B.V., Zakusin, S.V., Krupskaya, V.V., 2020. Quantitative methods for quantification of montmorillonite content in bentonite clays. *Georesursy* 22 (3), 38–47. <https://doi.org/10.18599/grs.2020.3.38-47>.
- Bogomazov, V.M., 1961. Stratigraphy and conditions of formation of pre-carbonaceous and coal-bearing deposits of the Carboniferous and Permian Minusinsk basin. In: *Questions of geology of coal-bearing deposits of the Asian part of the USSR*. - Moscow: Publishing house of the Academy of Sciences of the USSR, pp. 79–116. In Russian.
- Bujda'k, J., Komadel, P., 1997. Interaction of Methylene-blue with reduced charge montmorillonite. *J. Phys. Chem.* 101, 9065–9068. <https://doi.org/10.1021/jp9718515>.

- Dai, S., Ward, C.R., Graham, I.T., French, D., Hower, J.C., Zhao, L., Wang, X., 2017a. Altered volcanic ashes in coal and coal-bearing sequences: a review of their nature and significance. *Earth Sci. Rev.* 175, 44–74.
- Dai, Shifeng, Ward, Colin R., Graham, Ian T., French, David, Hower, James C., Zhao, Lei, Wang, Xibo, 2017b. Altered volcanic ashes in coal and coal-bearing sequences: a review of their nature and significance. *Earth-Sci. Rev. J.* 175, 44–74.
- Doebelin, N., Kleeberg, R., 2015. Profex: a graphical user interface for the Rietveld refinement program BGMN. *J. Appl. Crystallogr.* 48, 1573–1580.
- Dohrmann, R., Genske, D., Karmland, O., Kaufhold, S., 2012. Interlaboratory CEC and exchangeable cation study of bentonite buffer materials: I. Cu(II)-triethylenetetramine method. *Clay Clay Miner.* 60 (2), 162–175. <https://doi.org/10.1346/CCMN.2012.0600206>.
- Dorofeev, A.N., Bolshov, L.A., Linge, I.I., Utkin, S.S., Saveleva, E.A., 2017a. Strategic master-plan for research demonstrating the safety of construction, operation and closure of a deep geological repository for radioactive waste. *Radioact. Waste* 1, 19–26.
- Dorofeev, A.N., Bolshov, L.A., Linge, I.I., Utkin, S.S., Saveleva, E.A., 2017b. Strategic master plan for R&D demonstrating the safety of construction. In: *Operation and Closure of a Deep Geological Disposal Facility for Radioactive Waste*. Radioactive Waste, 1, pp. 32–41. In Russian.
- Drits, V.A., Besson, G., Muller, F., 1995. An improved model for structural transformations of heat-treated aluminous dioctahedral 2:1 layer silicates. *Clay Clay Miner.* 43 (6), 718–731.
- Drits, V.A., Lindgreen, H., Salyn, A.L., Ylagan, R., Mccarty, D.K., 1998. Semiquantitative determination of trans-vacant and cis-vacant 2:1 layers in illites and illite-smectites by thermal analysis and X-ray diffraction. *Am. Mineral.* 83, 1188–1198.
- Emmerich, K., Wolters, F., Kahr, G., Galagy, G., 2009. Clay profiling: the classification of montmorillonites. *Clay Clay Miner.* 57, 104–114. <https://doi.org/10.1346/CCMN.2009.0570110>.
- Ericsson, T., Wäppling, R., 1976. Texture effects in 3/2–1/2 Mössbauer spectra. *J. Phys. Colloq.* 37 (6), 719–723.
- Farmer, V.C., 1974. *Mineralogical Society of Great Britain and Ireland. The Infrared Spectra of Minerals*, p. 4. <https://doi.org/10.1180/mono-4>.
- Fedotov, A.N., 1996. Geological Additional Exploration of a Scale of 1: 200000 in the Minusinsk Depression at Abakanskaya Area (Abakanskaya) (Krasnoyarsk).
- Fontaine, F., Christidis, G.E., Yans, J., Hollanders, S., Hoffman, A., Fagel, N., 2020. Characterization and origin of two Fe-rich bentonites from Westerwald (Germany). *Appl. Clay Sci.* 187, 105444.
- GOST, 1989. 28177–89 Clays Molding Bentonite.
- Hower, J., Eslinger, E.V., Hower, M.E., Perry, E.A., 1976. Mechanism of burial metamorphism of argillaceous sediment: 1 Mineralogical and chemical evidence. *Bull. Geol. Soc. Am.* 87, 725–737.
- Huff, W.D., 2016. K-bentonites: a review. *Am. Mineral.* 101 (1), 43–70. <https://doi.org/10.2138/am-2016-5339>.
- Huff, W.D., Merriman, R.J., Morgan, D.J., Roberts, B., 1993. Distribution and tectonic setting of Ordovician K-bentonites in the United Kingdom. *Geol. Mag.* 130, 93–100. <https://doi.org/10.1017/S001675680002375X>.
- Iliina, O.A., Krupskaya, V.V., Vinokurov, S.E., Kalmykov, S.N., 2019. State-of-art in the development and use of clay materials as engineered safety barriers at radioactive waste conservation and disposal facilities in Russia. *Radioact. Waste* 4 (9), 71–84. <https://doi.org/10.25283/2587-9707-2019-4-71-84>.
- Kadir, S., Kulah, T., Erkoyun, H., Christidis, G.E., Arslanyan, R., 2019. Geology, mineralogy, geochemistry, and genesis of bentonite deposits in miocene volcano-sedimentary units of the balikisir region, Western Anatolia, Turkey. *Clay Clay Miner.* 67, 371–398.
- Kaufhold, S., Dohrmann, R., Ufer, K., Meyer, F.M., 2002. Comparison of methods for the quantification of montmorillonite in bentonites. *Appl. Clay Sci.* 22, 145–151. [https://doi.org/10.1016/S0169-1317\(02\)00131-X](https://doi.org/10.1016/S0169-1317(02)00131-X).
- Kim, A.G., 2011. Chapter 1 - Coal Formation and the Origin of coal fires. *Coal Peat Fires: A Global Perspect.* 1, 1–28. <https://doi.org/10.1016/B978-0-444-52858-2.00001-3>.
- Krupskaya, V.V., Biryukov, D.V., Belousov, P.E., Lekhov, V.A., Romanchuk, A.Yu., Kalmykov, S.N., 2018. The use of natural clay materials to increase the nuclear and radiation safety level of nuclear legacy facilities. *Radioact. Waste* 2 (3), 30–43.
- Krupskaya, V.V., Zakusin, S.V., Lekhov, V.A., Dorzhieva, O.V., Belousov, P.E., Tyupina, E.A., 2020. Buffer properties of bentonite barrier systems for radioactive waste isolation in geological repository in the nizhnekanskiy massif. *Radioact. Waste* 1 (10), 35–55 (In Russian). [10.25283/2587-9707-2020-1-35-55](https://doi.org/10.25283/2587-9707-2020-1-35-55).
- Lisyansky, A.V., Sheshikov, A.V., 1978. Argillite Deposit 10<sup>th</sup> Khutor. Report with the Calculation of Reserves of Clay Raw Materials for Drilling Fluids (In Russian).
- Lorenz, P., Meier, L., Kahr, G., 1999. Determination of the cation exchange capacity (CEC) of clay minerals using the complexes of copper (II) ion with triethylenetetramine and tetraethylenepentamine. *Clay Clay Miner.* 47, 386–388.
- Madejová, J., Komadel, P., 2005. Information available from infrared spectra of the fine fractions of bentonites. In: Klopogge, J.T. (Ed.), *The Application of Vibrational Spectroscopy to Clay Minerals and Layered Double Hydroxides*, The Clay Minerals Society, Aurora, CO, pp. 65–98.
- Madejová, J., Gates, W.P., Petit, S., 2017. IR spectra of clay minerals. *Develop. Clay Sci.* 8, 107–149. <https://doi.org/10.1016/B978-0-08-100355-8.00005-9>.
- Mironov, K.V., 1991. *Coal Geologist's Handbook*. Nedra, p. 363 (In Russ.).
- Molodtsov, V.A., Ignatova, V.P., 1975. Determination of the composition of exchange bases in saline soils. *Soil Sci.* 2, 123–127.
- Moore, D.M., Reynolds Jr., R.C., 1999. *X-ray Diffraction and the Identification and Analysis of Clay Minerals*, 2nd ed. Oxford University Press, Oxford, UK; New York, p. 378.
- Pokidko, P.V., 2019. Advantages and Disadvantages of Various Methods for Determining CEC of Bentonite Clays. In Russian. IGEM RAN, Moscow, pp. 59–61.
- Post, J.E., Bish, D.L., 1989. Rietveld refinement of crystal structures using powder X-ray diffraction data. *Rev. Mineral. Geochem.* 20, 277–308.
- Pozner, V.V., 1969. *Atlas of Lithological-Paleogeographical Map of the USSR (V. II)*.
- Reka, A.A., Anovskii, T., Bogoevski, S., Pavlovski, B., Boškovski, B., 2014. Physical-chemical and mineralogical-petrographic examinations of diatomite from deposit near village of Rozden, Republic of Macedonia. *Geologica Macedonica* 28, 121–126.
- Sabitov, A.A., Ruselik, E.S., Trofimova, F.A., Teterin, A.N., 2010. Russian bentonite: the current state and resource base development potential. *Mineral resources of Russia. Econ. Manag.* 5, 8–17 (In Russ.).
- Shestakova, O.E., 2010. Petrography, structure and genesis of fossil coals. *Bull. Kuzbass State Tech. Univer.* 1 (77), 3–10 (In Russ.).
- State balance of mineral reserves of the Russian Federation: Bentonite Clays (2018). Vol. 45.
- Vantelon, D., Montarges-Pelletier, E., Michot, L.J., Briois, V., Pelletier, M., Thomas, F., 2018. Iron distribution in the octahedral sheet of dioctahedral smectites. An Fe K-edge X-ray absorption spectroscopy study. *Phys. Chem. Miner.* 30, 44–53. <https://doi.org/10.1007/s00269-002-0286-y>.
- Vergunov, A.V., Arbutov, S.I., Eremeeva, V.V., 2020. Mineralogy, geochemistry and genesis of rare metal Zr-Nb-Hf-Ta-REE-Ga mineralization of the seam xxx of Minusinsk BASIN. *Izvestiya Tomskogo Politehnicheskogo Universiteta Inzhiring Georesursov.* 331 (7), 49–62. <https://doi.org/10.18799/24131830/2020/7/2718>.
- Winchester, J.A., Floyd, P.A., 1977. Geochemical discrimination of different magma series and their differentiation products using immobile elements. *Chem. Geol.* 20, 325–343. [https://doi.org/10.1016/0009-2541\(77\)90057-2](https://doi.org/10.1016/0009-2541(77)90057-2).
- Wojdyr, M., 2010. Fityk: a general-purpose peak fitting program. *J. Appl. Crystallogr.* 43, 1126–1128. <https://doi.org/10.1107/S0021889810030499>.
- Zhigarev, V.V., Korenev, V.V., 2019. Geology and zoning of qualitative characteristics of some deposits of bentonite clays in Russia. In: *Materials of Reports of Clays and Clay Minerals Conference*. IGEM RAN, Moscow, pp. 254–256. In Russian.
- Zviagina, B.B., McCarty, D.K., Srodonón, J., Drits, V.A., 2004. Interpretation of infrared spectra of dioctahedral smectites in the region of OH-stretching vibrations. *Clay Clay Miner.* 52 (4), 399–410. <https://doi.org/10.1346/CCMN.2004.0520401>.